Polypropylene Fiber-Based Strain-Hardening Cementitious Composites

*Bang Yeon Lee[1], Victor C. Li[2] and Yun Yong Kim[3]

[1] *School of Architecture, Chonnam National University, Gwangju 500-757, Korea*
[2] *Department of Civil and Environmental Engineering, University of Michigan, Ann Arbor, MI 48105, USA*
[3] *Department of Civil Engineering, Chungnam National University, Daejeon 305-764, Korea*
[1] *bylee@jnu.ac.kr,* [2] *vcli@umich.edu,* [3] *yunkim@cnu.ac.kr*

ABSTRACT

When strain-hardening cementitious composites (SHCCs) are applied to structural members that are subjected to high levels of deformation, the high ductility of the composites increases the safety of the structures. Polyvinyl alcohol and Polyethylene fibers have been successfully used in the manufacture

of SHCCs. This paper discusses the performance of composites supplemented with PP fiber. Type I cement and fly ash F were used as binding materials. The water-to-binder ratio was 0.23-0.25 (by weight), and the superplasticizer-to-binder ratio was 0.004-0.005. The amount of PP fiber used was 2 vol%. Polystyrene beads were also used to increase the tensile ductility of composites; these beads have a very weak bond with a cementitious matrix, so they behave as an artificial flaw under tensile loading. An anti-foamer was also tested to reduce the entrained air formation. Uniaxial tension testing was performed on coupon specimens measuring 100 mm × 75 mm × 12.5 mm for the purpose of characterizing the tensile behavior of composites. The test results show that high tensile strain capacities (3% to 6%) can be attained by employing high-strength PP fibers in cementitious composites.

1. INTRODUCTION

Strain-hardening cementitious composites (SHCCs) are a special class of high performance fiber reinforced cementitious composites; they have an extreme tensile strain capacity (TSC), which is typically more than 3%, but require only a moderate amount of fibers, typically less than 2 vol%.Therefore, SHCCs are considered a

---

[1] Assistant Professor
[2] Professor
[3] Associate Professor

promising construction material for improving the safety and durability of structures because they have a high level of ductility and controlled tight crack widths. Polyvinyl-Alcohol (PVA) and Polyethylene (PE) fibers have been successfully used in the manufacture of SHCCs (Li 1998; Li et al. 2002). In addition, polypropylene (PP) fiber has been used to improve the fire-resistant property of concrete exposed to high temperatures (Hoff et al. 2000; Zeiml et al. 2006; Bentz 2000) and to reduce the shrinkage cracking of concrete (Grzybowski and Shah 1990; Voigt et al. 2004; Naaman et al. 2005). PP fiber, however, has not been used to achieve high tensile ductility because its low tensile strength and hydrophobic property induce poor interfacial bonding properties. This paper presents the fresh and hardened properties of the SHCC supplemented with a newly developed high-strength PP fiber (Lhoneix et al., 2002, Yang, 2008, Ikai et al., 2010 should be cited).

2. DESIGN FRAMEWORK

The strain-hardening behavior of SHCCs is achieved through the formation of matrix multiple cracking. The fundamental requirement for matrix multiple cracking is that steady-state flat cracking occurs. This feature was first characterized for continuous aligned fiber-reinforced ceramics (Marshall and Cox 1988), and subsequently extended to discontinuous fiber-reinforced cementitious composites (Li and Leung 1992). The SHCC design micromechanics can be found in previous work (Li and Leung 1992; Lin and Li 1997; Li and Wang 2006).

To ensure steady-state cracking, the crack tip toughness, J_{tip}, must be less than the complementary energy, J_b. These values are calculated from the fiber bridging stress, σ, versus crack opening, δ, curve (Marshall and Cox 1988; Li and Wu 1992). They are expressed as follows:

$$J_b = \sigma_0 \delta_0 - \int_0^{\delta_0} \sigma(\delta)\,d\delta \geq J_{tip}, \tag{1}$$

$$J_{tip} = \frac{K_m^2}{E_m} = \int_0^{\delta_{ss}} \sigma(\delta)\,d\delta, \tag{2}$$

where σ_0 is the maximum bridging stress corresponding to the flat crack opening, δ_0; K_m is the matrix fracture toughness; and E_m is the matrix Young's modulus. Eq. (1) expresses the energy balance between the external work, which is the energy necessary to propagate the matrix crack, the energy dissipated by the bridging fibers, and crack tip energy absorption through matrix breakdown.

The fiber bridging stress versus crack opening relationship, $\sigma(\delta)$, is analytically derived on the basis of fracture mechanics, micromechanics, and probabilistic tools. In particular, the energetics of tunnel crack propagation along the fiber-matrix interface is used to model the debonding process of a single fiber from the surrounding cementitious matrix. After the debonding is complete, the fiber pullout stage begins; this stage is modeled as slip-hardening behavior. By these means, the full debonding-pullout process of a single fiber with a given embedment length is quantified as the fiber bridging force versus fiber displacement relation (Lin and Li 1997). Probabilistics is then

introduced to describe the randomness of fiber location and orientation with respect to a crack plane; this step is based on the assumption of a uniform random fiber distribution (Wang et al. 1990). The random orientation of the fibers also necessitates some accounting of the mechanics of the interaction between an inclined fiber and the matrix crack. Additionally, the snubbing coefficient, f, and strength reduction factor, f', are introduced to account for the interaction between the fiber and the matrix as well as the reduction of fiber strength when the fiber is pulled at an inclined angle. As a result, the $\sigma(\delta)$ curve is expressed as a function of the following micromechanics parameters: the fiber volume content, V_f; the fiber diameter, d_f; the fiber length, L_f; the fiber Young's modulus, E_f the matrix Young's modulus, E_m; the interface chemical bond, G_D; the interface frictional bond, τ_0; and the slip-hardening coefficient, β; and f and f'.

Apart from the energy criterion (Eq. (1)), another condition for pseudo-strain-hardening is that the matrix tensile cracking strength, σ_c, must not exceed the maximum fiber bridging strength σ_0 (Li and Leung 1992; Li and Wu 1992). Thus,

$$\sigma_c < \sigma_0 \tag{3}$$

where σ_c is determined by the matrix fracture toughness, K_m, and the pre-existing internal flaw size, c_0. While the energy criterion governs the crack propagation mode, the strength-based criterion (Eq. (3)) controls the crack initiation from material defect sites.

The steady-state cracking criterion ensures the occurrence of multiple cracking. However, the steady-state cracking criterion is not directly related to the density of multiple cracking, which is closely related to the ultimate strain capacity the material can achieve. The matrix pre-existing flaw size distribution and the matrix fracture toughness are the factors which determine the number of cracks that can be developed before the maximum fiber bridging stress (i.e. the peak value of the $\sigma(\delta)$ curve) is reached. The maximum fiber bridging stress imposes a lower bound of the critical flaw size, c_{mc}: thus, only flaws larger than c_{mc} can be activated and contribute to multiple cracking. The size
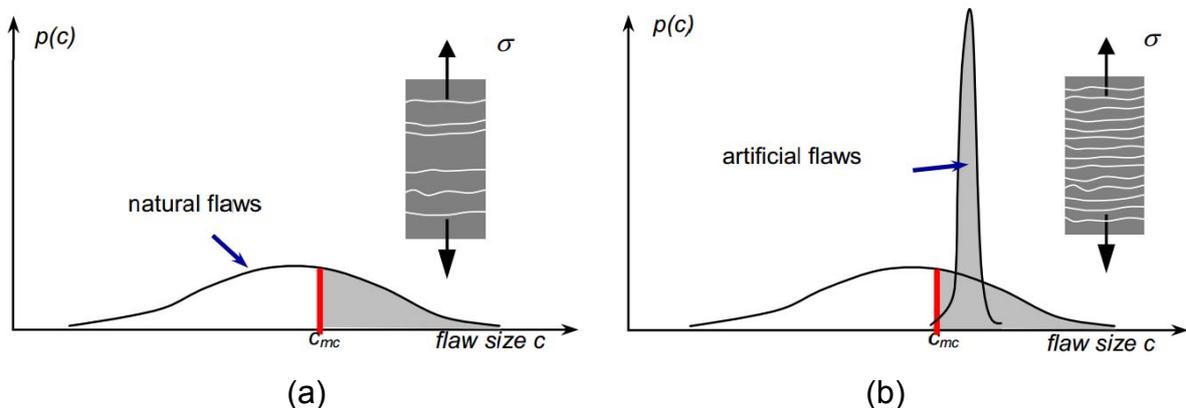

Fig. 1. Scheme of the flaw size tailoring for saturated multiple cracking in fiber reinforced brittle matrix composites: (a) natural flaw size distribution with random nature inherent from processing; (b) artificial flaws larger than critical size c_{mc} imposed to ensure saturation of multiple-cracking (Wang and Li 2004).

distribution of pre-existing flaws in matrix needs to be optimized to ensure the development of saturated multiple cracking and to obtain a high material strain capacity. Ideally, as illustrated in Fig. 1, these should be a narrow distribution above c_{mc}: a narrow distribution of this type may lead to a prolonged yielding plateau on the SHCC stress-strain curve (Wang and Li 2004). Smaller and larger flaws should both be avoided because the former cannot activate cracking and the latter deteriorate homogeneity of fiber distribution and reduce the tensile strength.

The conditions of strain-hardening and multiple cracking saturation indicate that a high material strain capacity requires a high J'_b value and a low J_{tip} value, as well as a sufficient number of pre-existing flaws larger than c_{mc}.

3. MATERIALS AND METHODS

3.1. Materials and mixture composition
The materials and mix proportions investigated in this study are listed in Table 1. ASTM Type I cement and ASTM C618 Class F normal fly ash (mean size: 17.5 μm) were used as cementitious-pozzolanic material. Polystyrene (PS) beads with a diameter of 4 mm and a density of 1.4 g/cm³ were used as artificial flaws. They are another type of aggregate that bonds in a very weak manner with a cementitious matrix, so they behave as artificial flaws under tensile loading. PS beads can serve as crack initiators because

Table 1. Mix proportions of PP fiber-based SHCCs

Mixture	Mix 1-1	Mix 1-2	Mix1-3	Mix 2-1	Mix 2-2	Mix 3-1
Cement	1	1	1	1	1	1
Fly ash F	2.8	2.8	2.8	2.8	2.8	2.8
PS bead*	0	0.092	0.046	0	0.092	0.092
Water	0.88	0.88	0.88	0.88	0.88	0.95
HRWRA**	0.016	0.016	0.016	0.018	0.018	0.014
Anti-foamer	0	0	0	0.0076	0.0076	0.0076
Fiber† (by vol.)	0.02	0.02	0.02	0.02	0.02	0.02

* Polystyrene (PS) beads
** High-range water-reducing admixture
† Brasilit high tenacity polypropylene

Table 2. Properties of PP fiber

Properties	Tensile strength (MPa)	Fiber diameter (μm)	Fiber length (mm)	Young's modulus (GPa)	Elongation (%)	Density (g/cm³)
PP fiber	850	12	10	6	21	0.91

they have sharp edges, and they bond in an extremely weak manner with the surrounding cement binder. An optimized amount of a high-range water-reducing admixture was used to achieve the proper rheology to ensure a uniform fiber dispersion and good workability. PP fiber (2 vol.%) was used as a reinforcement. The properties of the PP fiber used in this study are listed in Table 2.

The base mix proportion (Mix 1-1) of the composites was selected from the literature (Yang 2008). Mix 1-2, which is the same as Mix 1-1 except that it contains PS beads, was designed to evaluate the effect of artificial flaws. Mix 1-3, which is the same as Mix 1-2 except that it contains half the amount of PS beads, was designed to investigate how the amount of PS beads affects the TSC. Mix 2-1, which is the same as Mix 1-1 except that it contains an anti-foamer, was designed to eliminate undesirable air bubbles of the Mix 1-1 composite. Mix 2-2, which is the same as Mix 2-1 except that it contains PS beads, was designed to investigate how the inclusion of PS beads increases the TSC of Mix 2-1. Mix 3-1, which is the same as Mix 2-2 except that it has a high water content and a low SP content, was designed to increase the TSC of Mix 2-1 and to investigate how water-to-binder ratio affects on the TSC.

3.2. Mixing, casting, and curing of specimens

Each of the compositions was mixed in a Hobart mixer with 10L capacity. Solid ingredients, including cement and fly ash, were added to the mixer and mixed for approximately 3 min. Water was slowly added and the mixture was then mixed for another 3 min. Next, HRWRA and the anti-foamer, if required, were added into the mixer. Once a consistent mixture was reached, plastic beads, if required, were added and mixed for another 1 minute and then the fiber was gradually added. The whole mixing procedure for each batch generally took 10 min to 15 min. After the mixing, the mixture was cast into molds as a moderate vibration was applied. The molds were covered with plastic sheets and cured in air at room temperature (23°C ± 3°C) for 1 day. The hardened specimens were then removed from the molds and cured in air until 14 days or 28 days in a laboratory room at a temperature of 23°C ± 3°C. Along with the coupon specimens measuring 100 mm × 75 mm × 12.5 mm for the tension test, three 50 mm cubes (subjected to the same curing procedure) were cast for the purpose of measuring the compressive strength and density of the composite.

3.3. Flowability and density

Immediately after completion of mixing, the slump and slump flow were measured in accordance with ASTM C 143/C 143M and ASTM C 1611/C 1611 M. The densities of the cubes were measured after 1 day and the density value, ρ, were calculated as follows:

$$\rho = \frac{w_{\text{in AIR}}}{w_{\text{in AIR}} - w_{\text{in WATER}}} \times \rho_{\text{w}} \tag{4}$$

where $w_{\text{in AIR}}$ is the weight of the specimen in air and $w_{\text{in WATER}}$ is the weight of the specimen in water. ρ_{w} is the density of water (which is assumed to be 1 g/cm³).

3.4. Hardened properties

A compressive test system was used for the compression tests, which were conducted in a manner similar to ASTM C109. Three specimens were tested for each test series. Uniaxial tension testing was performed on coupon specimens to characterize the composite TSC and tensile strength. Before the commencement of the 28 day testing, aluminum plates were glued onto both ends of the coupon specimen to prevent of the specimen by gripping. The tests were conducted on an Instron load frame under a displacement control at a rate of 0.1 mm/min. The machine recorded the load values during the test; these values were used to calculate the tensile stress. Two external linear variable displacement transducers were attached to the surface of the specimen with the gauge length of 100 mm to measure the deformation of the specimen within the gauge length. The deformation value was used to calculate the tensile strain. For each test series, three or four specimens were tested at 14 days and 28 days.

4. RESULTS AND DISCUSSION

4.1. Flowability

Figure 2 shows the slump and slump flow values of the composites. The slump value is in the range of 178 mm to 267 mm, and the slump flow value is in the range of 356 mm to 540 mm. As expected, the flowability was improved by an increase of water and air bubbles. Figure 3 shows that the slump and slump flow values of Mix 1-2 are smaller than those of Mix 1-1. The same phenomenon can be observed in Mix 2-1 and Mix 2-2. These results indicate that the addition of PS beads decreases the slump and slump flow values; the decrease is mainly attributed to the fact that the PS beads absorb water and they may negatively affect the matrix workability due to their size. The flowability of Mix 3-1 is improved mainly because of the increased water-to-binder ratio.
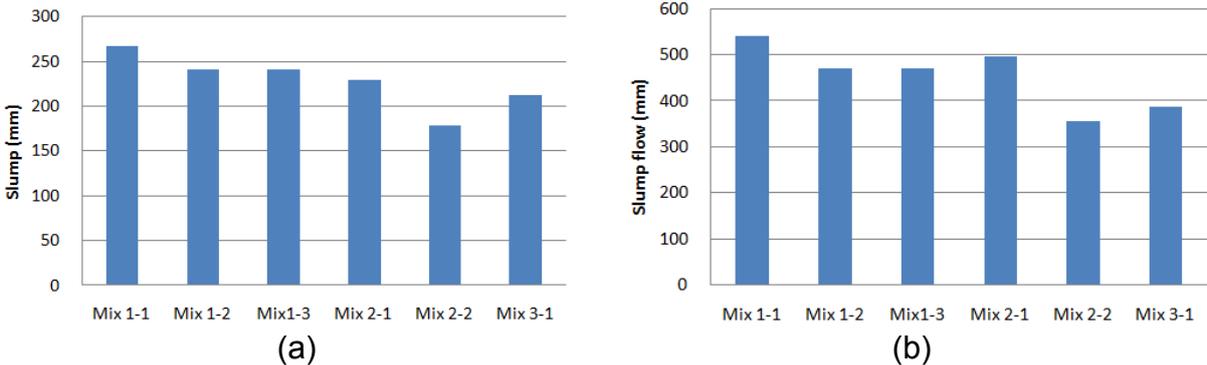

Fig. 2. Flowability: (a) slump and (b) slump flow

4.2 Density

Figure 3 shows the hardened density values of the composites. The composites without any anti-foamer (the Mix 1 series) have a density range of 1.22 to 1.31 g/cm³,

which is about 34% less than the theoretical density (1.91 g/cm³ to 1.95 g/cm³). This difference is attributed to the fact that many tiny air bubbles are homogeneously distributed throughout the composites (Fig. 4(a)). In contrast, the composites with the anti-foamer (the Mix 2 and Mix 3 series) have a density range of 1.68 g/cm³ to 1.78 g/cm³, which is close to the theoretical density of 1.9 g/cm³. The specimens of Mix 2 and Mix 3 series have normal amounts of air bubbles (Fig. 4(b)). The test results show that the density increases when the anti-foamer is added. On the other hand, the addition of PS beads for the creation of artificial flaws was observed to have a negligible effect on the density level.

Fig. 3. Density

| (a) | (b) |
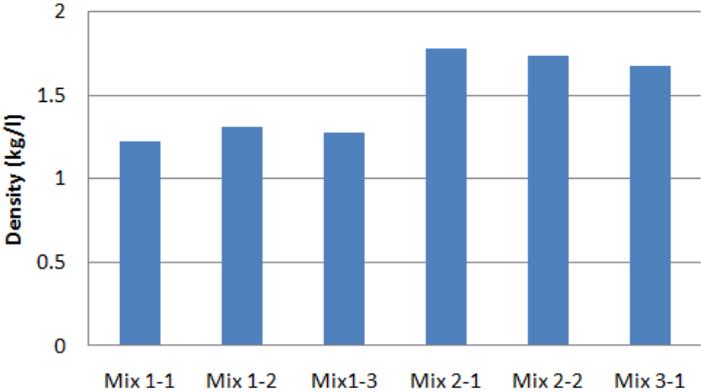
Fig. 4. Specimen surface; (a) Mix 1-1 (homogeneously distributed many tiny air bubbles); (b) Mix 2-1 (normal entrapped air bubbles)

4.3 Hardened properties
Figure 5 shows the tensile stress and strain curves of composites. As seen from the

tensile stress-strain curves, the ductility of Mix-1 and Mix-3 specimens were generally higher than that of Mix-2 specimens. The stress climbing behavior of curves with increasing strain was more significant in the case of Mix-3 specimens.
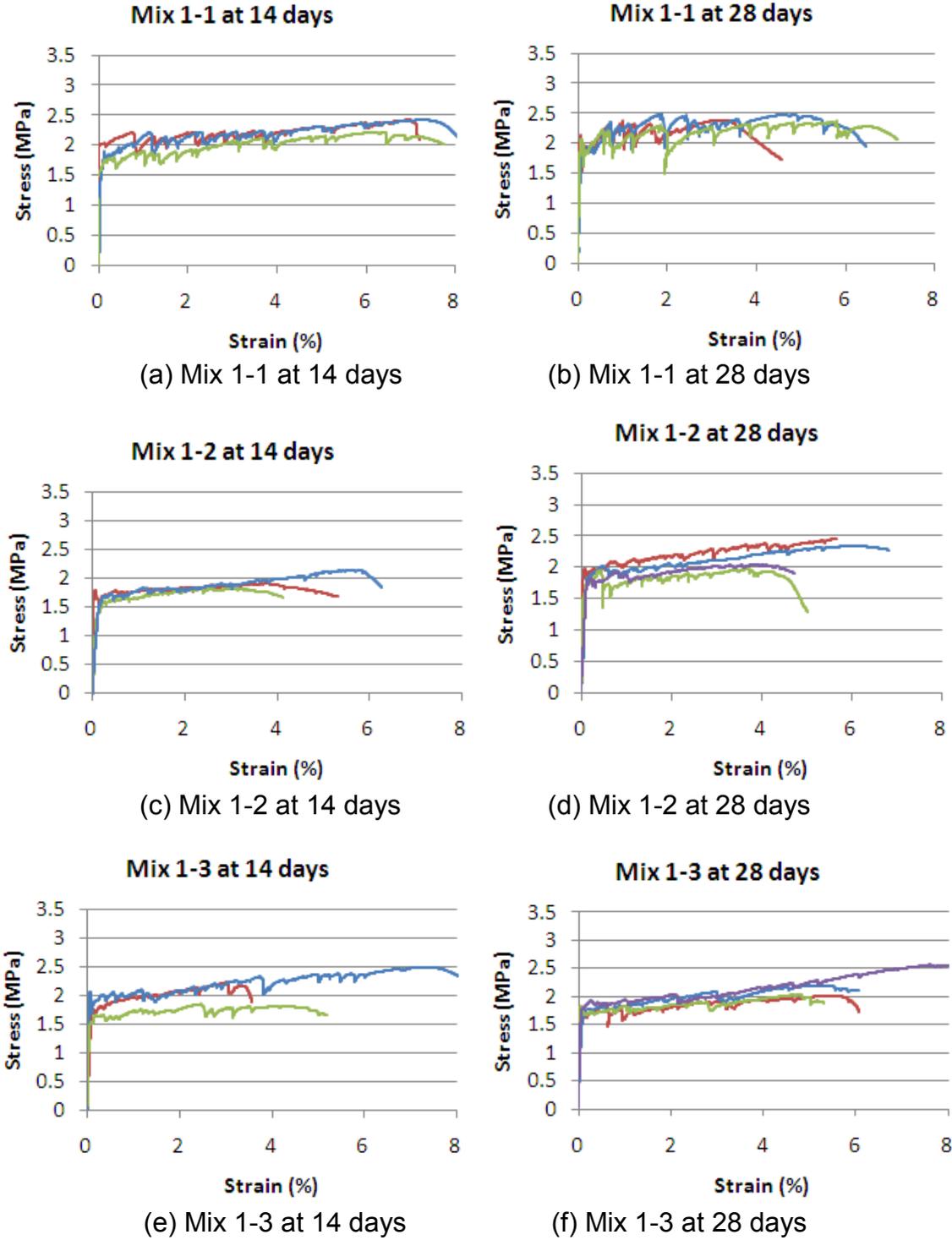

(a) Mix 1-1 at 14 days

(b) Mix 1-1 at 28 days

(c) Mix 1-2 at 14 days

(d) Mix 1-2 at 28 days

(e) Mix 1-3 at 14 days

(f) Mix 1-3 at 28 days

Fig. 5. Tensile stress and strain curves

(g) Mix 2-1 at 14 days   (h) Mix 2-1 at 28 days

(i) Mix 2-2 at 14 days   (j) Mix 2-2 at 28 days

(k) Mix 3-1 at 14 days   (l) Mix 3-1 at 28 days
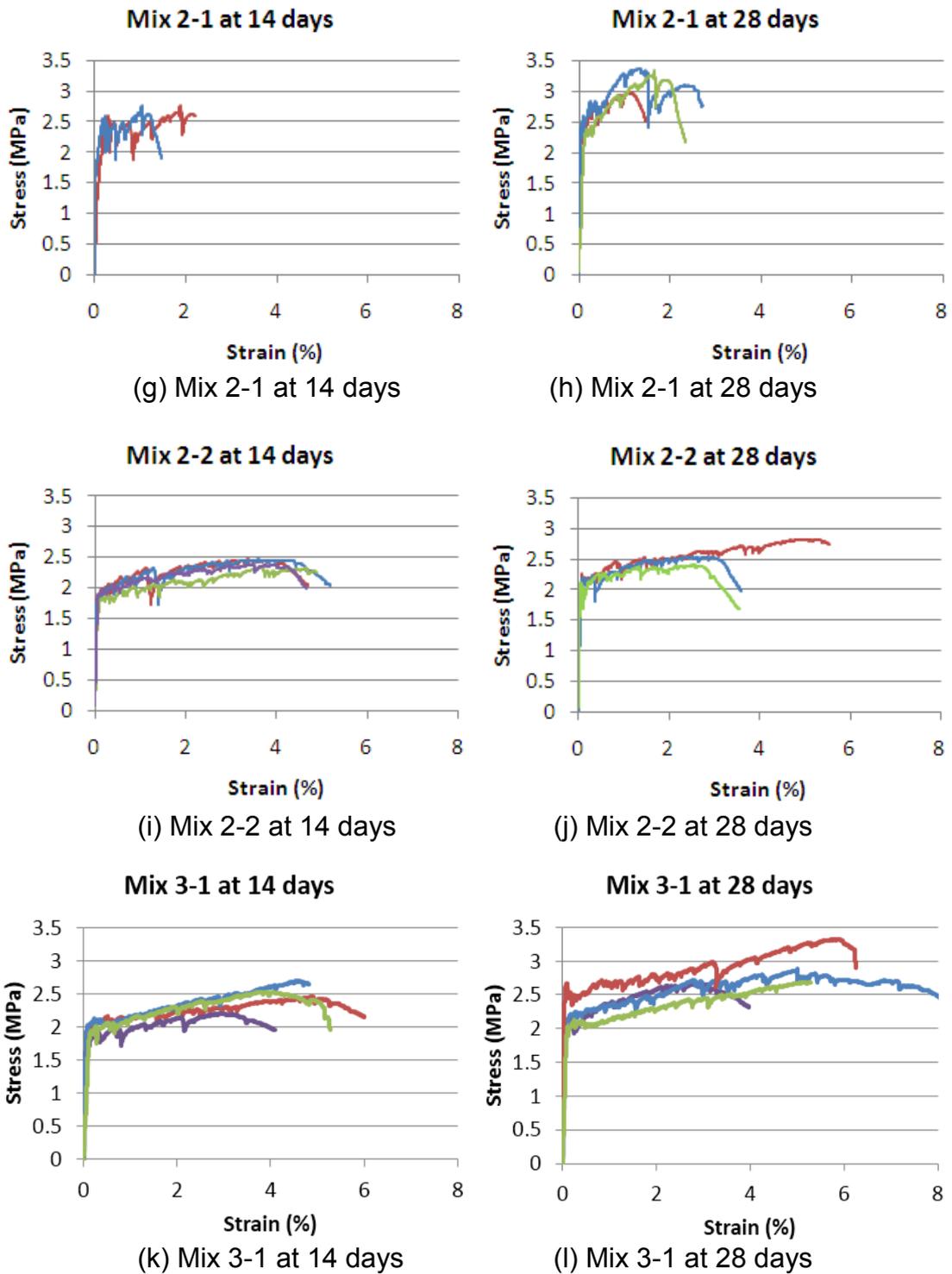
Fig. 5. Tensile stress and strain curves (continued)

Figure 6 shows the compressive strength of the composites. The compressive

strength of the composites without anti-foamer (the Mix 1 series) is in the range of 15.8 MPa to 18.7 MPa. On the other hand, the compressive strength of composites with the anti-foamer (the Mix 2) is about three times greater than that of the Mix 1 series. This difference is mainly attributed to the amount of air bubbles. The compressive strength of the Mix 3 series, the water-to-cement ratio of which is about 7% higher than that of the Mix 2 series, is about 16% lower than that of the Mix 2 series.
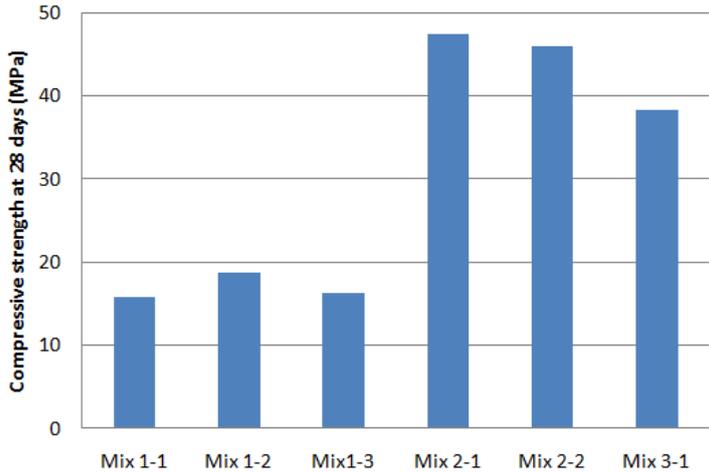

Fig. 6. Compressive strength at 28 days

Figure 7 shows the TSC values of the composites. The TSC of the Mix 1-1 was about 7% at 14 days and TSC of 4.5% at 28 days, with a high standard deviation. There was also a large variation in the TSC values of Mix 1-2 and Mix 1-3. PS beads were added to these two composites so that the resultant artificial flaws would reduce the large variation in the TSC of Mix 1-1 at 28 days. The limited tests of this study indicate that the addition of PS beads with 4 mm size is an ineffective means of reducing the variation in the TSC. Mix 1-3, which had only half the amount of PS beads used in Mix 1-2, has a higher TSC value than Mix 1-2, indicating that too many PS beads tend to reduce the fiber bridging capacity. Thirty two randomly selected cross sections (two for each specimen) of 16 specimens were investigated for the purpose of measuring the number of PS beads. An average of 4.6 (standard deviation: 2.2) PS beads was observed in the specimens of Mix 1-2, and an average of 2.5 (standard deviation: 1.3) PS beads was observed in the specimens of Mix 1-3. The TSC value of Mix 2-1 was 1.5% at 14 days and 1.3% at 28 days. In contrast, the TSC of Mix 2-2 was three times greater than that of Mix 2-1 at 14 days and at 28 days. This result is mainly attributed to the artificial flaws. Compared with Mix 2-2, Mix 3-1, which has a higher water-to-cement ratio, has almost the same TSC at 14 days and a 25.6% higher TSC at 28 days. This is mainly attributed to the lower K_m and the higher capillary porosity caused by an increase in w/c ratio.
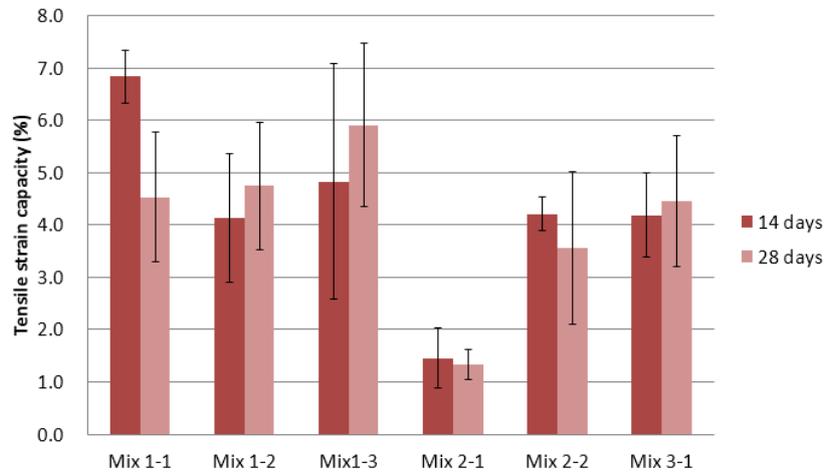
Fig. 7. Tensile strain capacity at 14 days and 28 days

Figure 8 shows the first cracking strength values at 28 days. Comparisons of Mix 1-1 and Mix 1-2 and of Mix 2-1 and Mix 2-2 reveal, firstly, that the addition of PS beads causes the first cracking strength to decrease by about 10% and, secondly, that the addition of anti-foamer causes the first cracking strength to increase by 25%. Increase in first crack strength due to the air bubble detraining effect of anti-foamer reduced the margin between first crack strength and ultimate strength values (Mix 1-1 compared to Mix 2-1). Due to this reason, TSC of Mix 2-1 composites decreased dramatically. The addition of plastic beads somewhat reduced this effect (Mix 2-2). The average first cracking strength of Mix 3-1 is similar to that of Mix 2-2. The limited tests of this study confirm that the first cracking strength is affected less by the water-to-cement ratio than the amount of PS beads.
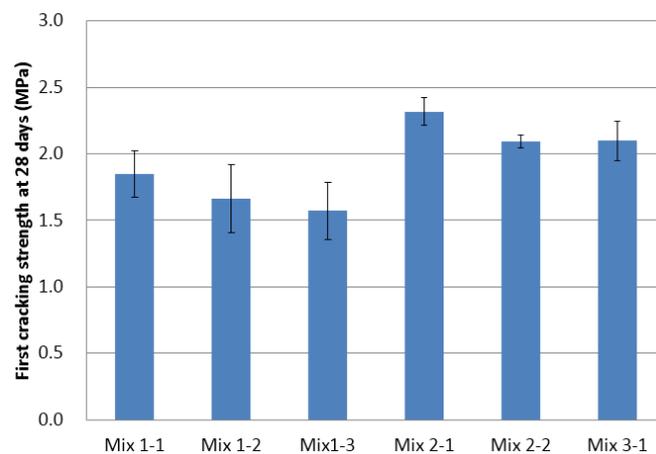

Fig. 8. First cracking strength at 28 days

Figure 9 shows the ultimate strength values at 28 days. The ultimate tensile strength of Mix 1-2 and Mix 1-3 was, on average, about 8.2% less than that of Mix 1-1. In addition, the ultimate tensile strength of Mix 2-2 was 22.9% less than that of Mix 2-1 because the addition of PS beads lowered the fiber bridging capacity.
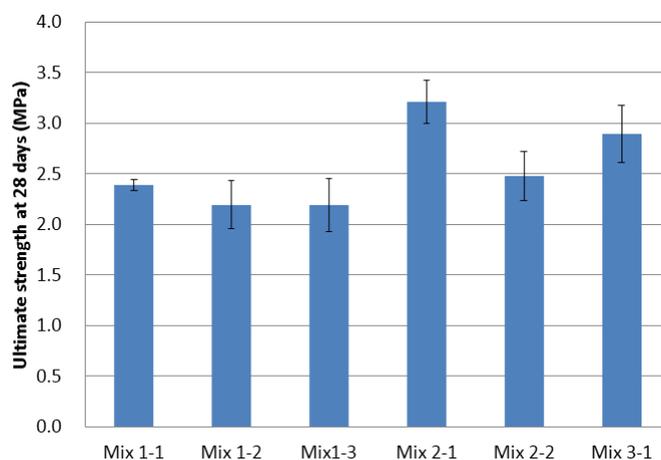

Fig. 9. Ultimate strength at 28 days

5. CONCLUSION

This paper discusses the performance of three kinds of cementitious composites supplemented with high strength PP fibers. A series of experimental tests was performed to characterize the fresh and hardened properties of the composites. The following conclusions can be drawn from the current results:

(1) Cementitious composites using PP fibers, designed based on mechanics and statistical theory, show high tensile ductility as much as PVA or PE fiber based SHCC.
(2) PP fiber based cementitious composites showed the slump of 178~267 mm, slump flow of 356~540 mm and the density of 1.22~1.78 kg/*l*.
(3) PP fiber based cementitious composites showed the tensile strain capacity of 3~6%, along with the first cracking strength of 1.6~2.1 MPa, the ultimate strength of 2.2~2.8 MPa and the compressive strength of 15~45 MPa. While tensile strength values are comparable with normal strength concrete, these new composites are significantly more ductile with at least 300 times higher TSC.
(4) From the hardened property tests, it was verified that artificial flaws can be very effective to increase the average TSC of composites. This improvement can be linked to the higher margin between first crack and ultimate strength. However, the variation in the TSC remained unchanged.

REFERENCES

Bentz, D.P. (2000) "Fibers, Percolation, and Spalling of High Performance Concrete," *ACIMaterials Journal,* Vol. **97**(3), 351-359.

Grzybowski, M., and Shah, S. P. (1990) "Shrinkage Cracking of Fiber Reinforced Concrete,"*ACI Materials Journal*, **87**(2), 138-148.

Hoff, G.C., Bilodeau, A., and Malhotra, V.M. (2000) "Elevated Temperature Effects on HSC Residual Strength," *Concrete International*, **22**(4), 41-48.

Ikai, S., Reichert, J.R., Vasconcellos, A.R., Zampieri, V.A. (2006) "Asbestos-Free Technology With New High Tenacity PP - Polypropylene Fibers In Air-Cured Hatschek Process," *IIBCC*, Universidade de Sao Paulo & University of Idaho: Sao Paulo– Brazil, November 15-18, pp.33-48

Lhoneux, B. de, R. Kalbskopf, P. Kim, V. C. Li, Z. Lin, D. Vidts, S. Wang, and H .C. Wu (2002). "Development of High Tenacity Polypropylene Fibers for Cementitious Composites," *Proceedings of the JCI International Workshop on Ductile Fiber Reinforced Cementitious Composites (DFRCC) - Application and Evaluation* (*DRFCC-2002*), Takayama, Japan, Oct., pp.121-132.

Li, V.C. (1998) "Engineered Cementitious Composites – Tailored Composites through Micromechanical Modeling," in Fiber Reinforced Concrete: Present and the Future, edited by N. Banthia, A. Bentur, A. and A. Mufti, Canadian Society for Civil Engineering, Montreal, 64-97.

Li, V. C.; Leung, C. K. Y. (1992) "Steady-State and Multiple Cracking of Short Random Fiber Composites," *ASCE J Engrg Mech.*, **118**(11), 2246-2264.

Li, V.C., and Wang, S. (2006) "Microstructure Variability and Macroscopic Composite Properties of High Performance Fiber Reinforced Cementitious Composites," *Probabilistic Engineering Mechanics*, **21**(3), 201-206.

Li, V.C., and Wu, H.C. (1992) "Conditions for Pseudo Strain Hardening in Fiber Reinforced Brittle Matrix Composites", *Journal of Applied Mechanics Review*, **45**(8), 390-398.

Li, V.C., Wu, C., Wang, S., Ogawa, A., and Saito, T. (2002) "Interface Tailoring for Strain-Hardening Polyvinyl Alcohol-Engineered Cementitious Composite (PVA-ECC)," *ACI Materials Journal*, **99**(5), 463-472.

Lin, Z. and Li, V.C. (1997) "Crack Bridging in Fiber Reinforced Cementitious Composites with Slip-hardening Interfaces," *J. Mechanics and Physics of Solids*, **45**(5), 763-787.

Marshall, D. B.; Cox, B. N. (1988): A J-integral method for calculating steady-state

matrix cracking stressed in composites. *Mechanics of Materials,* **7**(2), 127-133.

Naaman, A. E., Wongtanakitcharoen, T., and Hauser, G. (2005) "Influence of Different Fibers on Plastic Shrinkage Cracking of Concrete," *ACI Materials Journal*, **102**(1), 49-58.

Voigt, T., Bui, V. K., and Shah, S. P. (2004) "Drying Shrinkage of Concrete Reinforced with Fibers and Welded-Wire Fabric," *ACI Materials Journal*, **101**(3), 233-241.

Wang, Y., Backer, S., and Li, V.C. (1990) "A Statistical Tensile Model of Fiber Reinforced Cementitious Composites," *Journal of Composites*, **20**(3), 265-274.

Wang, S. and Li, V. C. (2004) "Tailoring of Pre-existing Flaws in ECC Matrix for Saturated Strain Hardening," Proceedings of FRAMCOS-5, Vail, Colorado, U S A, 1005-1012.

Yang, E.H. (2008) "Designing added functions in engineered cementitious composites," The University of Michigan, Ph. D. Thesis.

Zeiml, M., Leithner, D., Lackner, R., and Mang, H.A. (2006) "How Do Polypropylene Fibers Improve The Spalling Behavior of In-Situ Concrete?," *Cement and Concrete Research*, **36**(5), 929-942.